JACS
JOURNAL OF THE AMERICAN CHEMICAL SOCIETY
Article
pubs.acs.org/JACS
Terms of Use

In Situ NMR Spectroscopy of Supercapacitors: Insight into the Charge Storage Mechanism

Hao Wang,[†,‡,∥] Alexander C. Forse,[†,∥] John M. Griffin,[†] Nicole M. Trease,[‡] Lorie Trognko,[§] Pierre-Louis Taberna,[§] Patrice Simon,[§] and Clare P. Grey*[,†,‡]

[†]Department of Chemistry, University of Cambridge, Lensfield Road, Cambridge CB2 1EW, U.K.
[‡]Department of Chemistry, Stony Brook University, Stony Brook, New York 11794-3400, United States
[§]Université Paul Sabatier Toulouse III, CIRIMAT, UMR-CNRS 5085, F-31062 Toulouse, France

Supporting Information

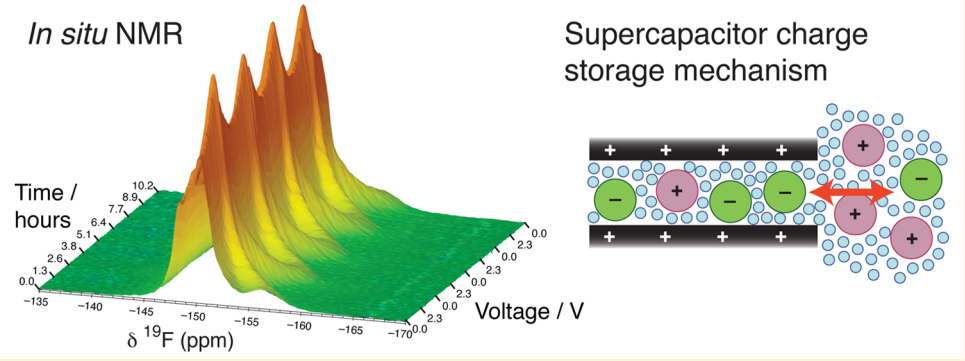

ABSTRACT: Electrochemical capacitors, commonly known as supercapacitors, are important energy storage devices with high power capabilities and long cycle lives. Here we report the development and application of in situ nuclear magnetic resonance (NMR) methodologies to study changes at the electrode−electrolyte interface in working devices as they charge and discharge. For a supercapacitor comprising activated carbon electrodes and an organic electrolyte, NMR experiments carried out at different charge states allow quantification of the number of charge storing species and show that there are at least two distinct charge storage regimes. At cell voltages below 0.75 V, electrolyte anions are increasingly desorbed from the carbon micropores at the negative electrode, while at the positive electrode there is little change in the number of anions that are adsorbed as the voltage is increased. However, above a cell voltage of 0.75 V, dramatic increases in the amount of adsorbed anions in the positive electrode are observed while anions continue to be desorbed at the negative electrode. NMR experiments with simultaneous cyclic voltammetry show that supercapacitor charging causes marked changes to the local environments of charge storing species, with periodic changes of their chemical shift observed. NMR calculations on a model carbon fragment show that the addition and removal of electrons from a delocalized system should lead to considerable increases in the nucleus-independent chemical shift of nearby species, in agreement with our experimental observations.

1. INTRODUCTION

The development of efficient energy storage devices is essential to meet the growing demand for portable electronic devices and emerging green transportation technologies. While lithium ion batteries have met a large proportion of our needs over the past 20 years, electrochemical capacitors, also known as supercapacitors, are receiving renewed interest as an alternative and complementary technology.[1] The storage of electrical energy in carbon-based supercapacitors relies on the formation of an electric double-layer at the interface between a solid electrode and a liquid electrolyte solution. This non-faradaic charge storage mechanism allows rapid rates of charge and discharge and essentially unlimited cycle lives, making supercapacitors well-suited to high power applications.[2,3]

Supercapacitors typically use organic electrolytes, such as tetraethylammonium tetrafluoroborate (NEt_4BF_4) in acetonitrile.[1] Aqueous electrolytes are also sometimes used because they are less toxic and inexpensive; however, the decomposition of water at voltages above 1.2 V limits the amount of energy that can be stored. Supercapacitor electrodes are generally constructed using porous carbon owing to its high surface area and conductivity.[4] In particular, activated carbons derived from organic precursors such as coconut shells and wood have been widely used in commercial devices owing to their high surface area and conductivity, and low cost. Although predominantly microporous (with pore sizes less than 2 nm), these materials also exhibit a range of pore diameters in the mesoporous (2−50 nm diameter) and macroporous (greater than 50 nm diameter) regimes. The importance of pore size effects was highlighted by

Received: October 11, 2013
Published: November 25, 2013

   dx.doi.org/10.1021/ja410287s | J. Am. Chem. Soc. 2013, 135, 18968−18980

Chmiola et al., who reported that the capacitance of carbon derived from titanium carbide dramatically increased when the average size of carbon micropores was less than the size of the solvated electrolyte ions (typically less than 1.5 nm).[5] This finding could not be explained with traditional concepts of double-layer formation and has triggered considerable efforts toward understanding the nature of ion electrosorption inside the porous carbon. It was hypothesized that ion desolvation allowed a closer approach of charge centers at the electrode−electrolyte interface.[6] Distortions of cyclic voltammograms in cavity microelectrode studies confirmed that electrolyte ions are at least partially desolvated as they enter the carbon micropores upon charging.[7] However, many questions relating to this phenomenon and the fundamental mechanism of supercapacitance in general remain unanswered.

A deeper understanding of the processes that take place within supercapacitors upon charging and discharging will enable further development and optimization of these important devices. To this end, a number of experimental methods have been employed to further investigate the behavior of ions in micropores.[8] In situ electrochemical quartz crystal microbalance (EQCM) methodologies have been used to study the gravimetric response of porous carbon electrodes in a range of electrolyte systems under dynamic charging conditions. Deviations from theoretical mass changes have been interpreted in terms of distinct charging regimes that are characterized by the compositional differences in the ionic part of the electric double layer.[9−12] Small-angle neutron scattering measurements have been used to observe changes in the concentration of electrolyte ions in micropores as a function of applied potential,[13] while neutron diffraction has been employed to quantify the diffusion of ions within mesoporous carbons in different charge states.[14] Recently, an in situ infrared spectroscopy method has been developed to study supercapacitor systems.[15] Decreases in electrolyte ion absorbances were interpreted as arising from a net movement of positive and negative ion pairs into carbon micropores upon charging.[15] In addition to experimental work, a large number of theoretical studies have given insight into charging phenomena in supercapacitors. In particular, molecular dynamics simulations[16−22] have shown the importance of overscreening effects at planar electrode−electrolyte interfaces, whereby the first layer of adsorbed species encompasses more charge than the electrode surface itself, with subsequent layers of electrolyte ions balancing the overall charge at the interface. It has been suggested that the absence of such effects in microporous electrodes allows high capacitances to develop.[23] Further work based on mean field theory models has proposed that image forces arising from charged micropore surfaces facilitate the packing of ions of the same polarity during charging, accounting for the large increases in capacitance experimentally measured for carbons with micropores smaller than the solvated electrolyte ions.[24−26]

While experimental and theoretical work has advanced the understanding of charge storage in porous carbons, further development is required to directly observe and quantify changes of ion environments in supercapacitor electrodes. Nuclear magnetic resonance (NMR) spectroscopy is a powerful technique for studying electrochemical interfaces, as the observed resonance frequency is sensitive to the local chemical environment. This approach is also element selective, allowing the separate observation of different chemical species in electrochemical systems. The potential of NMR to study adsorption of molecules on carbon was recognized in early work by Harris et al. where distinct resonances were observed for adsorbed and non-adsorbed species within activated carbons.[27−30] More recent work on adsorption on a variety of different carbon morphologies has revealed similar trends.[31−39] Regardless of the molecule or nuclear spin studied, resonances from species adsorbed on a given carbon show similar shifts to low frequencies, relative to the nonadsorbed species. This suggests that the observed shift is a nucleus-independent chemical shift (NICS), arising from aromatic ring current effects associated with delocalized π electrons in the carbon. In addition to experimental NMR methods for probing this phenomenon, computational approaches have been developed to calculate NICSs arising from delocalized systems.[40,41] Such calculations have been applied to a range of carbon systems including coronenes,[42] fullerenes,[43,44] nanotubes,[45−47] and graphene.[47]

In addition to studies of adsorption within porous carbons with no applied potential, NMR can also be used to study the charging and discharging mechanisms of supercapacitors. Indeed, NMR uniquely allows the direct observation of the charge storing species (adsorbed species). Ex situ NMR[48−50] involves holding a supercapacitor at a particular voltage, disassembling it, and then acquiring the NMR spectrum of the electrolyte species that remain inside the electrode film. With this approach, magic angle spinning (MAS) can be used to improve resolution and identify subtle changes in ion environments.[50] However, the rapid evaporation of acetonitrile during disassembly can result in the solidification of electrolyte salt. Desorption of ions (or self-discharge) during disassembly may also make it difficult to know exactly how much charge is stored when an NMR spectrum is acquired.

In situ NMR experiments[51−55] can address some of the issues associated with ex situ approaches, since spectra of the working device are acquired directly. Such experiments offer direct insight into the behavior of working devices but come with some resolution losses due to the incompatibility with MAS techniques. Our previous in situ NMR study demonstrated the utility of NMR for the study of supercapacitors during charging (and discharging), and systematic changes were observed in the spectra.[32] ^{11}B NMR experiments were used to probe the behavior of BF_4 anions at different applied cell potentials. It was shown that the adsorption processes occurring at each electrode could be studied separately by introducing a prototype long supercapacitor design. Changes in populations and resonance frequencies were observed for adsorbed BF_4 anions upon cell charging. However, the electrochemical properties of the long supercapacitor cell were not fully explored, and while clear changes in both the local environments and populations of the adsorbed anions were observed, the link between these and the supercapacitor charging mechanism was not studied in detail.

In this work, in situ NMR is further developed to study supercapacitors comprising activated carbon electrodes and a NEt_4BF_4 in acetonitrile electrolyte. We first address some of the practical aspects associated with in situ NMR of supercapacitors, using ^{19}F NMR in this study because of the high sensitivity of this nucleus. We then show how this methodology can provide insight into the charge storage mechanism of supercapacitors by directly tracking changes in the amount of charge storing species as a function of applied voltage and identifying different charge storage regimes in a high surface area, coconut-derived activated carbon. Supercapacitor charging

is also shown to have a marked effect on the local magnetic environment experienced by adsorbed species. Real-time NMR experiments with simultaneous cyclic voltammetry show a systematic variation of the observed resonance frequency of adsorbed species, which is directly correlated with the development of charge on the electrodes. This is supported by NICS calculations on a model graphene fragment that show that the addition or removal of electrons from carbon systems has significant effects on the resonance frequencies of adsorbed species.

2. EXPERIMENTAL SECTION

2.1. Materials. In this work all carbon electrodes were prepared from YP50F carbon (Kuraray Chemical, Japan). Film electrodes were prepared in the standard way[56] by mixing carbon powder (95 wt %) with polytetrafluoroethylene (5 wt %) (Sigma Aldrich, 60 wt % dispersion in water). Prior to sample preparation, carbon film pieces (6.0 mg, approximate dimensions of 10 mm × 4 mm × 0.25 mm) were dried under vacuum at 200 °C overnight and then transferred to an argon glovebox. In initial electrochemical tests of different cell designs, the electrolyte used was a 1.5 M solution of tetraethylammonium tetrafluoroborate (NEt_4BF_4, Sigma Aldrich, electrochemical grade >99.0%) in acetonitrile (Sigma Aldrich, 99.8% anhydrous). This electrolyte is referred to as NEt_4BF_4/ACN. The same electrolyte was used for NMR experiments except that the solvent was replaced by deuterated acetonitrile, D_3CCN (Euriso-top, 99.96%). We refer to this electrolyte as NEt_4BF_4/dACN.

2.2. Sample Preparation. All sample preparation was carried out in an argon glovebox. Model electrodes were prepared for preliminary experiments by hermetically sealing a carbon film piece (6.0 mg) inside a plastic bag (3M packaging film) with the chosen volume of NEt_4BF_4/dACN electrolyte, which was added using a microsyringe. All supercapacitors in this study employed plastic bag cell designs, modified from Bellcore's plastic lithium ion battery technology.[53] Two pieces of carbon film (6.0 mg) were adhered to carbon-coated aluminum mesh, and a Cellgard 2500 (monolayer polypropylene, 25 μm thickness) separator was placed between them. These components were placed inside a plastic bag (3M packaging film), which was hermetically sealed on three sides. The cell was then saturated with electrolyte before making the final seal to close the bag. For NMR measurements, the supercapacitor bag cells were held between two plastic inserts in order to provide rigidity and allow better control over the cell orientation inside the NMR coil.

2.3. Electrochemical Tests. All cells were tested on a Bio-logic cycler or an Arbin Instruments battery cycler with a two-electrode configuration. Cyclic voltammetry (CV) was used both to test the performance of different cells and to run real-time in situ NMR experiments. Fixed voltage in situ NMR experiments were performed using chronoamperometry (CA) experiments. A fixed cell voltage is applied and a current flows around the external circuit until equilibrium is achieved before NMR acquisition.

2.4. NMR Details. All NMR experiments were performed using a Bruker Avance spectrometer operating at a magnetic field strength of 7.05 T, corresponding to a ^{19}F Larmor frequency of 284.2 MHz with a Bruker HX double resonance static probe using a 6.8 mm inner diameter solenoid coil. ^{19}F NMR spectra were referenced relative to neat hexafluorobenzene (C_6F_6) at −164.9 ppm. The "depth" pulse sequence[57] was used to acquire all ^{19}F NMR spectra in order to reduce the background signal from the PTFE probe-head housing. The total delay between excitation of transverse magnetization and acquisition of the free induction decay was 60 μs in all cases. Spectral fitting was carried out using dmfit software.[58] The minimum number of components required to obtain a satisfactory fit was found to be four for each electrode. For the positive electrode, deconvolutions were carried out assuming the free electrolyte feature to be made up of three purely Lorentzian components and assuming the strongly adsorbed feature to be made up of a single purely Gaussian component. For the negative electrode, much better fits were obtained assuming two Lorentzians and one Gaussian component for the free electrolyte and assuming a Gaussian line shape for the strongly adsorbed resonance. That more than one resonance is required to model the free electrolyte is ascribed to bulk magnetic susceptibility (BMS) effects and strong variations in local magnetic fields across the bag cell, which results in a range of different local fields and thus shifts for the same chemical species (see Supporting Information, Figure S3). For the spectra of the negative electrode, the shift of the strongly adsorbed resonance was first obtained by fitting spectra recorded with a short recycle interval (0.5 s) which favors observation of the strongly adsorbed resonance due to faster spin−lattice, T_1, relaxation. The shifts obtained were then fixed in the fits of the quantitative spectra recorded with the longer recycle interval of 30 s. For each electrode, the spectrum obtained at 0 V was fitted first, as this showed the best resolution of the strongly adsorbed resonance. The peak positions and intensities obtained were then used as a starting point to fit the spectrum at the next highest voltage. For the positive and negative electrodes, spectra recorded above 1.5 and 1.25 V, respectively, were not fitted, as unique fits could not be obtained owing to the almost complete overlap of the strongly adsorbed and free electrolyte features. Deconvoluted spectra are shown in Supporting Information, Figure S1.

2.5. In Situ NMR Experiments. Prior to performing NMR experiments, the cell was cycled between 0 and 2.3 V five times by cyclic voltammetry at a sweep rate of 0.5 $mV{\cdot}s^{-1}$. The positively charged electrode was first positioned inside the coil for detection, and the cell was charged sequentially to a series of different voltages (0, 0.25, 0.5, 0.75, 1, 1.25, 1.5, 1.75, and 2 V). The cell was held at each voltage for 40 min to ensure that an equilibrium charge state was attained before ^{19}F NMR spectra were acquired. After the positively charged electrode was studied, the cell was shifted to position the negatively charged electrode inside the NMR coil for detection. The cell was then charged to the same series of voltages, and ^{19}F NMR spectra were collected at each voltage after waiting for 40 min. For fixed voltage experiments, a recycle interval of 30 s was sufficient for spectra to be quantitative. ^{19}F NMR spectra were also collected while simultaneous cyclic voltammetry (CV) was performed on the cell. Unless otherwise stated, 94 NMR spectra were obtained per full CV cycle (0 V → 2.3 V → 0 V) with a recycle interval of 3 s. While this does not yield fully quantitative spectra, it reduces the time required to obtain each spectrum, enabling more spectra to be acquired during the CV cycle.

2.6. Calculations. All geometry optimizations and NMR calculations were performed using Gaussian 03 software.[59] First, geometries were optimized at the B3LYP level of theory with the 6-31G(d) basis set, as in other work.[42] Then an NMR calculation was performed at the same level of theory and with the same basis set to evaluate the chemical shielding tensors for each atom, as well as for several "ghost" atoms introduced around the structure. These ghost atoms have no electrons or nuclear charge and simply serve to act as probes of the local effective magnetic field at their position. The calculations generate the isotropic chemical shielding, σ_{iso}. The isotropic nucleus-independent chemical shift, δ_{iso}^{NICS}, is given by $-(\sigma_{iso} - \sigma_{ref})$, where σ_{ref} is a reference shielding which has a value of 0 ppm in this case.

3. RESULTS AND DISCUSSION

3.1. Cell Design for NMR Studies. Here, we considered three different supercapacitor cell designs in order to compare their electrochemical performances. The "conventional" design (Figure 1a) represents a typical supercapacitor, with the two electrodes situated directly on top of each other. With this design, both electrodes must be placed inside the NMR coil during in situ NMR experiments, making it difficult to separate processes occurring at each electrode.[32] In the "long" cell design (Figure 1b) the electrodes are shifted laterally with respect to each other so that a single electrode can be placed in the NMR detection region. In our previous work, this allowed

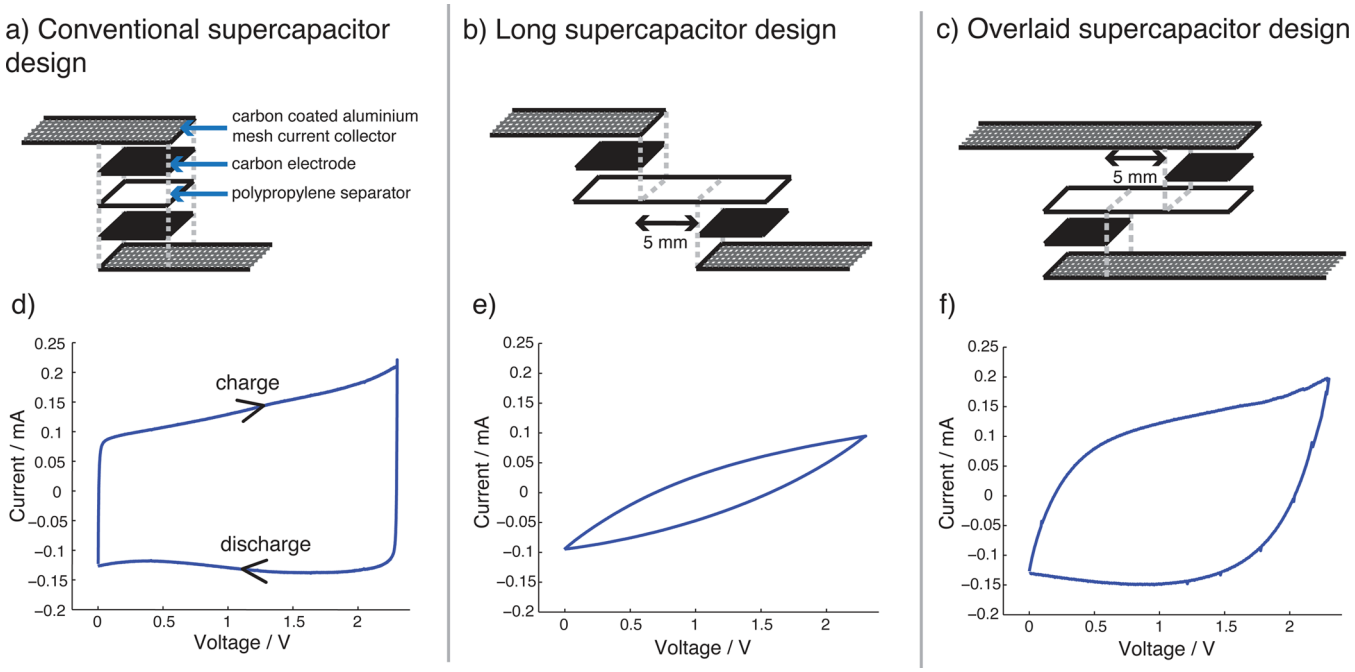

Figure 1. Supercapacitor cell designs (a–c) and their cyclic voltammograms at 0.5 mV·s^{-1} (d–f). In each case the cyclic voltammogram of the fourth cycle is shown.

the anion environments to be tracked separately in the positive and negative electrodes, although long times were needed to charge and discharge the device because of the significant ohmic losses associated with this design.[32] The "overlaid" cell design introduced here (Figure 1c) also allows a single electrode to be placed in the NMR detection region, but the current collector of the opposite electrode is situated closer to the electrode under study.

Cyclic voltammograms for conventional, long, and overlaid supercapacitors, each cycled at 0.5 mV·s^{-1} between 0 and 2.3 V, are shown in parts d, e, and f of Figure 1, respectively. Each cell comprised two YP50F film electrodes (6.0 mg each) and was saturated with NEt_4BF_4/ACN electrolyte (~30 μL for the conventional design and ~50 μL for the long and overlaid designs). A rectangular cyclic voltammogram is expected for an ideal capacitor, with positive currents flowing in the charge part of the cycle and negative currents flowing in the discharge part of the cycle. Distortion from the rectangular shape arises because of the contribution of resistive components associated with ionic diffusion, as well as the contact between the current collector (carbon coated aluminum mesh in our design) and the carbon electrode. A characteristic near-rectangular shape is observed for the conventional supercapacitor (Figure 1d), whereas the long cell design displays far from ideal behavior (Figure 1e), and a plateau indicative of pure capacitive behavior is not observed. However, a considerable improvement is achieved by switching to the overlaid design, where the observed cyclic voltammogram is much closer to the ideal case (Figure 1f). We also note that the estimated capacitance of YP50F (calculated from the discharge current at 1 V) is 99 F·g^{-1}, which is in good agreement with the literature value of 95 F·g^{-1}.[60] Faster scan rates were also studied for the long and overlaid cells, but poorer electrochemical performance was observed (see Figure S2 in Supporting Information). Importantly, the overlaid design introduced here allows a single electrode to be placed inside the NMR detection region while maintaining good electrochemical performance. Therefore, the overlaid design was used for all in situ NMR experiments that follow in this work, and a sweep rate of 0.5 mV·s^{-1} was used for cyclic voltammetry experiments.

3.2. Effect of Supercapacitor Components on the NMR Spectrum. In this work we focus on ^{19}F NMR to study the BF_4^- electrolyte anion environments. While ^{1}H NMR is an attractive option to study the environments of the NEt_4^+ cations, the large number of plastic components used in the bag cell assembly results in a broad and intense background ^{1}H signal that precludes the observation of the relatively low intensity electrolyte resonances. Before carrying out in situ ^{19}F NMR measurements on working supercapacitor cells at different applied potential differences, the form of the spectrum observed for an overlaid supercapacitor was investigated by comparison with model carbon film electrodes soaked with electrolyte. Figure 2a shows the static ^{19}F NMR spectrum obtained for a piece of YP50F carbon film (6.0 mg) soaked with 8 μL of NEt_4BF_4/dACN electrolyte, sealed inside a plastic bag. This carbon film piece represents a model electrode, with no applied potential difference. As in our previous studies, two main environments are observed.[31,32] The feature at −158.0 ppm is assigned to the electrolyte anions strongly adsorbed on carbon surfaces inside micropores. The feature at −152.4 ppm is assigned to weakly adsorbed anions, situated further from carbon surfaces and occupying spaces in large carbon pores and spaces between primary carbon particles in the carbon film. The −5.6 ppm shift of the strongly adsorbed relative to the weakly adsorbed feature is attributed to ring current effects arising from the delocalized electrons in the carbon. On increasing the amount of electrolyte in the sample to 15 μL (Figure 2b), the intensity of the weakly adsorbed resonance is increased. A small additional feature is also observed at higher frequency due to the presence of free electrolyte external to the carbon film piece.

dx.doi.org/10.1021/ja410287s | J. Am. Chem. Soc. 2013, 135, 18968−18980

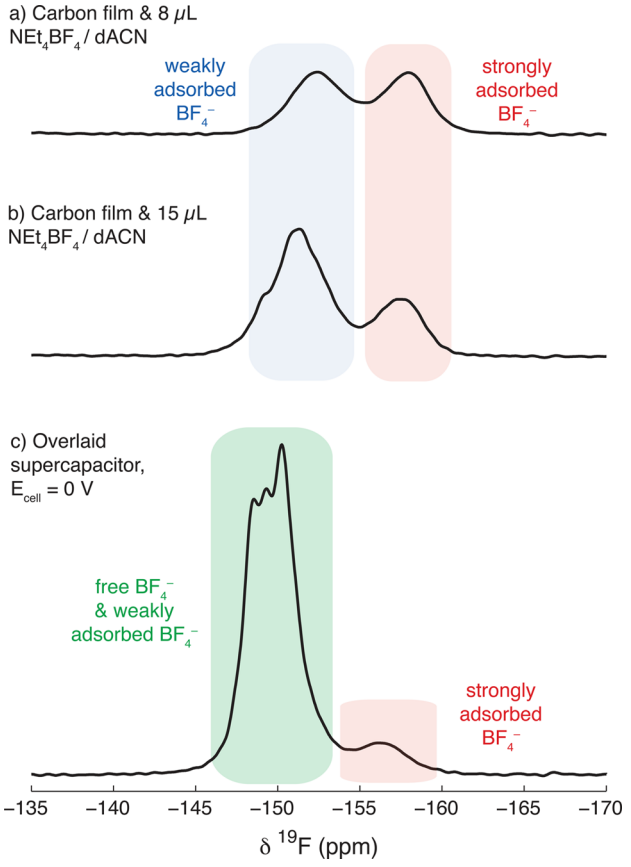

Figure 2. ^{19}F NMR spectrum obtained for pieces of carbon film soaked with (a) 8 μL and (b) 15 μL of NEt_4BF_4/dACN electrolyte. (c) Spectrum obtained for an overlaid supercapacitor held at a cell voltage of 0 V. The films were orientated vertically inside the NMR coil to enhance resolution of spectral features.[31] All spectra are shown on the same scale.

Figure 2c shows the NMR spectrum for an overlaid supercapacitor cell held at a cell voltage of 0 V. Here a single electrode is placed inside the NMR detection region. Again the strongly adsorbed electrolyte anions can be observed, appearing at −156.2 ppm. In addition, several more intense features corresponding to the weakly adsorbed anions and anions in free electrolyte external to the carbon electrode are observed at higher frequencies. This is due to the larger amount of electrolyte used in the supercapacitor cell to ensure good electrochemical performance. We note that the free electrolyte signal appears to comprise at least three superimposed components. Bag cell samples containing just free electrolyte (and current collector and free electrolyte) gave similar spectral features (see Supporting Information Figure S3). We attribute this to bulk magnetic susceptibility (BMS) effects owing to the irregular shape of the sample contained within plastic bag cells. Indeed, NMR spectra of isotropic substances contained within nonspherical samples have been shown to be complex, especially for flat orientated samples.[61,62] It is also noted that all the features in this spectrum are shifted to higher frequency by approximately 2 ppm relative to their counterparts in Figures 2a and 2b. Previous studies have shown that anisotropic BMS effects can be significant when studying flat electrode assemblies by NMR.[31,52,63] For the spectra shown in Figure 2, care was taken to ensure all samples were oriented vertically inside the NMR coil; however, the geometry and dimensions of the overlaid supercapacitor cell are intrinsically different to the soaked carbon film samples, and therefore, it is likely that the observed ∼2 ppm difference in chemical shift arises from BMS effects relating to the anisotropic shape of the sample and from the presence of a second current collector in the NMR coil. Importantly, despite the intense feature arising from the large amount of free electrolyte in the plastic bag cell, the spectra show that the strongly adsorbed ions are clearly evident in the NMR spectrum of an overlaid supercapacitor at zero potential and can be observed separately from the weakly adsorbed and free electrolyte features. Thus, with this design, changes in the anion environments may be tracked as a function of applied potential.

3.3. In Situ ^{19}F NMR Spectroscopy at Fixed Voltages.

To investigate changes to the BF_4 anion environments as a function of applied potential, ^{19}F NMR spectra of a single supercapacitor electrode were acquired while the cell was held at different voltages. Previous studies have indicated that small irreversible changes attributed to ion trapping or surface reactions can take place in supercapacitors during the first few charging cycles.[64] For this reason, the supercapacitor cell was cycled 5 times by cyclic voltammetry prior to being studied by NMR. First the positive electrode (and the surrounding electrolyte) was studied, with spectra shown in Figure 3a. At 0 V, the strongly adsorbed feature is observed at −156.5 ppm and the intense free electrolyte signal is observed between −148 and −150 ppm. As the voltage is increased from 0 to 2 V, the strongly adsorbed feature shows gradual increases in resonance frequency (the peak shifts toward the left-hand side of the spectrum), shown more clearly in the inset in Figure 3a. This feature also appears to show small but significant increases in intensity as the cell voltage is increased. The weakly adsorbed and free electrolyte features do not display significant changes in resonance frequency upon charging. After the positive electrode was studied, the supercapacitor cell was shifted so that the negatively charged electrode was situated in the NMR detection region, and the ^{19}F NMR spectra at various applied cell voltages are shown in Figure 3b. This was done to maintain the same polarity of the device and reduce any possible ion trapping effects.[64] At 0 V, a spectrum similar to that in Figure 3a is observed, with the strongly adsorbed feature visible at −154.9 ppm. We note that this feature is approximately 1.5 ppm higher in frequency than was observed for the positive electrode at 0 V. This suggests that cycling of the cell prior to acquisition of the NMR spectra results in small differences in the equilibrium states for the two electrodes. BMS effects are also expected to result in small shift differences, since different electrodes (with slightly different sizes and orientations relative to the applied magnetic field) are investigated. As the voltage is increased from 0 to 2 V, the strongly adsorbed feature again shifts to higher frequency, as was observed in the positive electrode (Figure 3a). However, here changes in the intensity of the strongly adsorbed feature appear to be less pronounced as the feature moves to higher frequency.

To aid with the interpretation of the results shown in Figure 3, spectra were deconvoluted to quantify the position and intensity of the strongly adsorbed resonance at each voltage. Details of the deconvolution procedure are given in the Experimental Section and Supporting Information. Deconvolutions were not performed for spectra acquired above 1.5 V (positive electrode) and 1.25 V (negative electrode), as the overlap between the strongly and weakly adsorbed features precluded accurate fitting. Figure 4a and Figure 4b show the

dx.doi.org/10.1021/ja410287s | J. Am. Chem. Soc. 2013, 135, 18968−18980

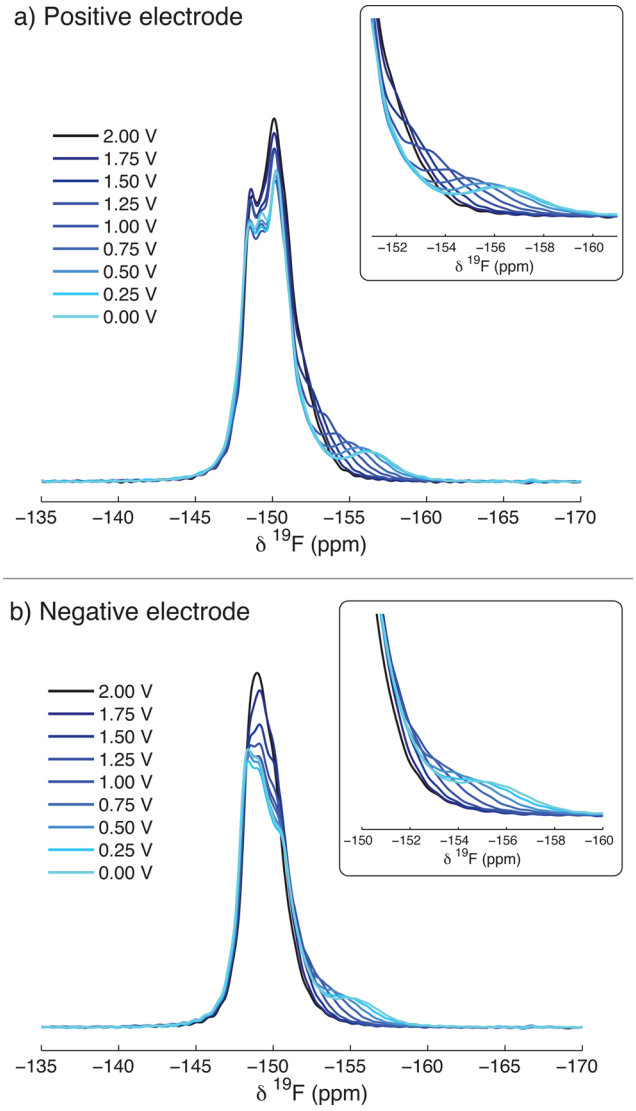

Figure 3. (a) ^{19}F NMR spectra of the positively charged electrode of an overlaid cell at voltages between 0 and 2 V. (b) ^{19}F NMR spectra of the negatively charged electrode of the same cell at voltages between 0 and 2 V. Insets show enlarged sections of the spectra to illustrate changes of the strongly adsorbed feature.

fitted intensity of the strongly adsorbed resonance for the positive and negative electrodes, which in each case are normalized to the intensity measured for each electrode at 0 V. For the positive electrode, at cell potentials between 0 and 0.75 V, the intensity of the adsorbed resonance does not change significantly. However, between 0.75 and 1.5 V a relatively sharp increase in intensity is observed. For the negative electrode, the intensity of the adsorbed resonance is found to decrease steadily over the voltage range studied. We note that the exact changes in intensity depend upon the fitting procedure used for the deconvolutions, which is not straightforward owing to the complexity of the spectra. However, deconvolutions performed using a different fitting procedure (see Supporting Information Figures S4 and S5) also show similar trends whereby a pronounced increase in the intensity of the adsorbed resonance is observed for the positive electrode at potentials higher than 0.75 V, and an approximately constant decrease in the intensity of the adsorbed resonance is observed for the negative electrode over the voltage range studied. The deconvoluted integrated intensities of the weakly adsorbed and free electrolyte features were not found to change significantly in either electrode over the voltage range studied (as shown in Supporting Information Figure S6). However, interpretation of the intensities of these features is not straightforward, since only part of the cell is situated inside the NMR detection region. This makes it difficult to distinguish intensity changes resulting from rearrangement of ions within the electrodes and changes resulting from diffusion of ions in and out of the NMR detection region.

From integration of the current relaxation, the total charge stored in the supercapacitor was found to increase approximately linearly with applied voltage (see Supporting Information Figure S7). The quantification of strongly adsorbed BF_4 anions in the positive and negative electrodes therefore offers insight into the fundamental mechanism underlying the charging process in this system. For the positive electrode, two distinct charging regimes can be identified. At voltages lower than 0.75 V, the almost constant intensity of the strongly adsorbed feature indicates that the charge storage process does not involve significant changes in the number of adsorbed anions. This suggests that the mechanism of charge storage in this low-voltage regime is dominated by short-scale ion rearrangement and/or the ejection of NEt_4 cations from the micropores. Indeed, recent molecular dynamics simulations have shown that local rearrangements of ions within porous carbon play an important role in supercapacitor charging.[65] At voltages higher than 0.75 V, the abrupt increase in intensity of the strongly adsorbed feature shows that BF_4^- anions are adsorbed into the micropores and that this plays a more significant role in charge storage in this regime. For the negative electrode, the intensity of the strongly adsorbed feature decreases approximately linearly over the range studied. In principle, the loss of BF_4 anions from the micropores should leave an excess of cations within the micropores to counteract the negative charge developed in the electrode. These results are in qualitative agreement with conclusions drawn from EQCM measurements on a similar porous carbon with a NEt_4BF_4/propylene carbonate electrolyte.[10] For this system, mass changes that are lower than expected on the basis of Faraday's law were observed at low charge densities and were explained in terms of anion−cation mixing within the micropores. At intermediate charge densities, mass changes close to the theoretical value were observed, indicating that the adsorption of counterions dominates the charge storage process. Our observation of an apparent "threshold" voltage of 0.75 V, whereby an abrupt increase in the strongly adsorbed resonance intensity is observed, may be related to the different charging regimes identified by the EQCM approach.

Figure 4c shows how the chemical shift of the strongly adsorbed resonance varies in the positively charged electrode as the cell voltage is increased. Clear increases in chemical shift are observed for the strongly adsorbed anions as the voltage is increased. While only small increases are observed between 0 and 0.5 V, at higher voltages an approximately linear trend is seen. As the cell voltage is increased from 0 to 1.5 V, a total increase in chemical shift of 3.9 ppm is measured. At voltages above 1.5 V, the strongly adsorbed peak appears to shift to higher frequencies still (Figure 3a), although this precludes reliable fitting of the spectra because of increased overlap of spectral features. In Figure 4d the chemical shift of the strongly adsorbed resonance for the negatively charged electrode is

dx.doi.org/10.1021/ja410287s | J. Am. Chem. Soc. 2013, 135, 18968−18980

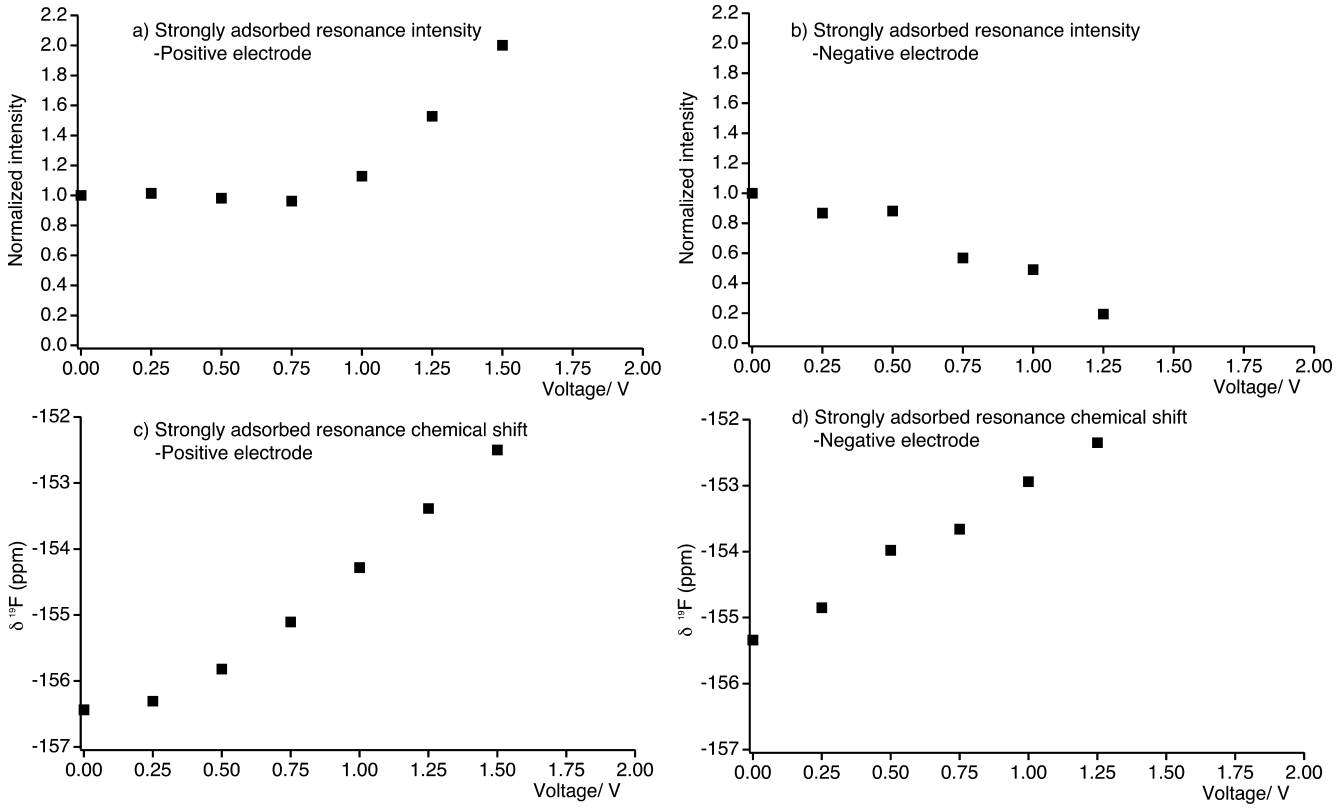

Figure 4. Summary of deconvolution results of spectra shown in Figure 3. Panels a and b show intensities of the strongly adsorbed feature in the positive and negative electrodes, each normalized by the intensity of this feature in the 0 V spectrum. Panels c and d give the deconvoluted chemical shift values for the strongly adsorbed feature in the positive and negative electrodes, respectively. It was not possible to obtain unique fits for spectra corresponding to voltages above 1.5 and 1.25 V for the positive and negative electrodes, respectively.

shown as a function of applied cell voltage. Again, clear increases in chemical shift are observed. Here, the chemical shift appears to vary in a linear fashion as the cell voltage is increased. As the voltage is increased from 0 to 1.25 V, the chemical shift increases from −155.3 to −152.4 ppm, representing a total increase of 2.9 ppm. This change is very similar to the overall change in resonance frequency of 3.0 ppm for the strongly adsorbed resonance in the positive electrode over the same voltage range. However, the change in resonance frequency for the negative electrode appears to be approximately linear over the range studied, whereas the positive electrode displays a nonlinear change in resonance frequency at low voltages.

In both the positive and negative electrodes, clear increases in the chemical shift of the resonances corresponding to strongly adsorbed BF_4 anions are observed as the supercapacitor is charged. This shows that the local environment of the anions changes during supercapacitor charging. We previously reported similar observations in a ^{11}B in situ NMR study of a highly analogous supercapacitor system.[32] When the BF_4 anion was probed, ^{11}B in situ NMR experiments revealed increases in the chemical shift of adsorbed species in both electrodes as the supercapacitor was charged. Furthermore, recent ^{11}B and ^{13}C ex situ studies of supercapacitors comprising activated carbon electrodes and a NEt_4BF_4/ACN electrolyte revealed similar increases in the chemical shift of adsorbed features upon charging.[50] In that study two activated carbons different from the one studied here were investigated, suggesting that the chemical shift variations we have observed are general phenomena.

3.4. Real-Time in Situ ^{19}F NMR Spectroscopy. To study the behavior of a working supercapacitor in more detail, in situ NMR spectra were recorded in real time for an overlaid supercapacitor undergoing simultaneous cyclic voltammetry. ^{19}F NMR spectra were collected while the cell was cycled between 0 and 2.3 V at a rate of 0.5 $mV{\cdot}s^{-1}$, with spectra acquired for four full electrochemical cycles. Since the cell voltage is being changed continuously, small changes of ∼0.05 V occur during the acquisition of one NMR spectrum. Since this change is small (2%) compared to the full cycling window of 2.3 V, we may approximate the voltage to be constant during the acquisition of one NMR spectrum. Figure 5a shows selected ^{19}F NMR spectra of the positive electrode extracted at different points from the cyclic voltammogram of the second cycle, shown as an inset. Spectra corresponding to voltages of 0, 0.5, 1, 1.5, and 2 V are shown. The spectrum acquired at 0 V shows a form very similar to the spectrum of the positive electrode for a fixed (static) voltage of 0 V shown in Figure 3a, with the strongly adsorbed resonance observed at −156.3 ppm. For spectra obtained at later stages in the charging cycle, the strongly adsorbed feature is observed to shift to higher frequencies, in good agreement with the fixed voltage behavior shown in Figure 3a.

The NMR spectra shown in Figure 5a represent a small selection of the total acquired NMR data. Indeed, 94 ^{19}F NMR spectra were obtained for each full 0 → 2.3 → 0 V cycle, with four full cycles studied. In Figure 5b, NMR spectra for all four electrochemical cycles are shown in a three-dimensional plot. The same spectra are displayed in the first video file in Supporting Information. This plot reveals a highly periodic

dx.doi.org/10.1021/ja410287s | J. Am. Chem. Soc. 2013, 135, 18968−18980

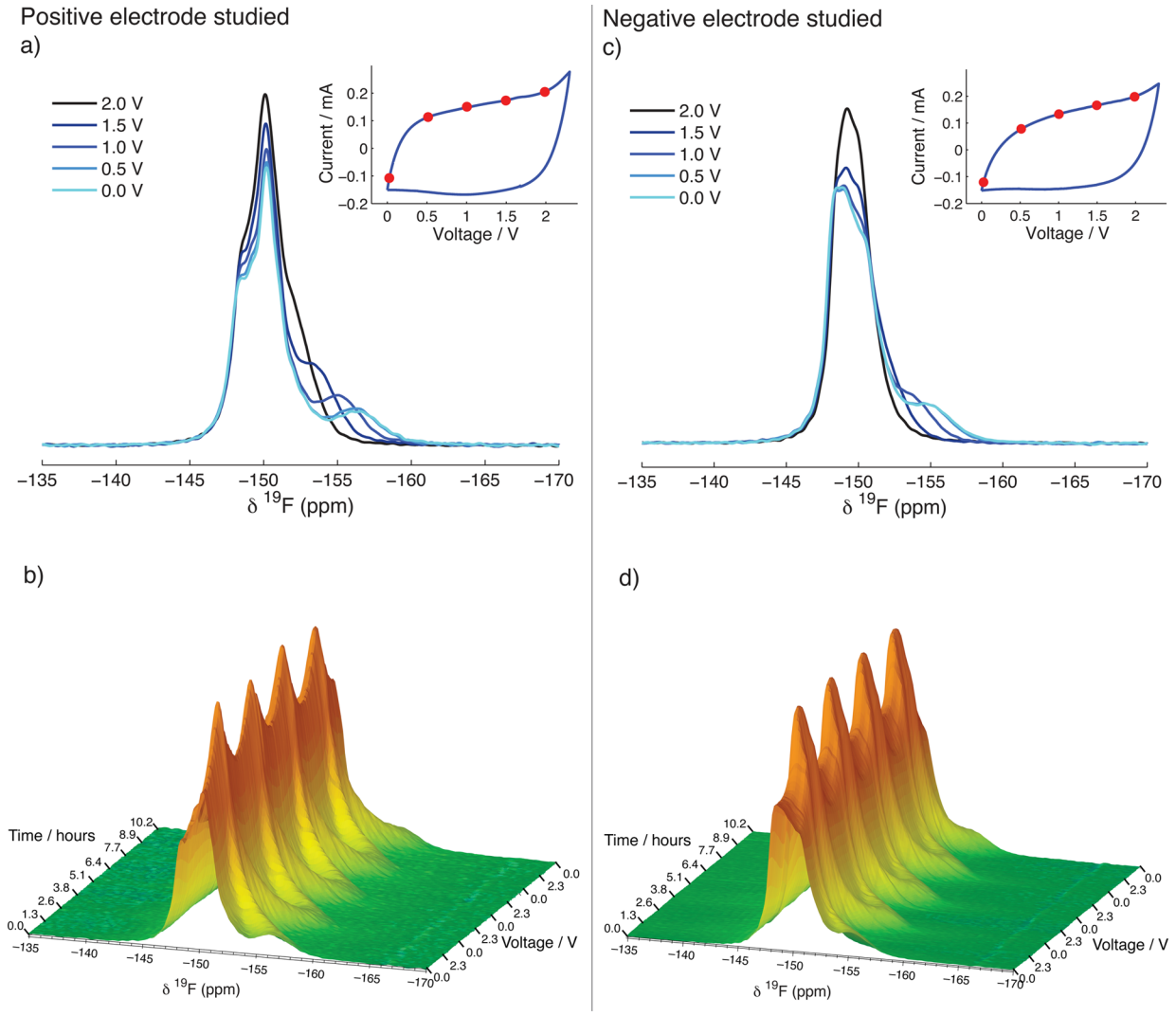

Figure 5. (a) Selected ^{19}F NMR spectra of the positive electrode of an overlaid capacitor cycled by cyclic voltammetry. Spectra are extracted from the charge during the second cycle. (b) Successive NMR spectra from four full cyclic voltammetric cycles are shown back to back. (c, d) Analogous results for the negative electrode of the supercapacitor cell are shown.

variation of the adsorbed resonance, the frequency of which varies in almost perfect correlation with the applied voltage. During the charging part of the cycle, the adsorbed resonance shifts to higher frequency, moving underneath the free electrolyte feature. During the discharging part of the cycle, the adsorbed resonance moves back to lower frequency until it reaches −156.3 ppm at 0 V. Over each 0 V → 2.3 V → 0 V cycle, a total change in frequency of ∼3.5 ppm is observed.

The real-time in situ experiment was repeated with the supercapacitor cell shifted so that the negative electrode occupied the NMR detection region. NMR spectra of the negative electrode extracted from the charge of the second electrochemical cycle are shown in Figure 5c. Again, for the spectrum acquired at 0 V the strongly adsorbed environment is clearly visible at approximately −155.1 ppm. As the cell voltage is successively increased to 2.3 V, the strongly adsorbed peak shifts to higher frequency. In Figure 5d, the full set of real-time in situ NMR spectra for the negative electrode is presented as a three-dimensional plot (spectra can also be seen in the second video file in Supporting Information), where again the periodic shifting of the strongly adsorbed environment is clearly observed.

The highly periodic behavior observed for the shift of the adsorbed resonance in both electrodes indicates that changes in the chemical shift originate from a reversible process, directly related to the charging and discharging of the supercapacitor electrode. Further insight into this phenomenon can be obtained by comparing real-time in situ NMR spectra acquired at different electrochemical cycling rates. Real-time in situ ^{19}F NMR spectra recorded during electrochemical cycling at rates of 0.5 and 5 mV·s^{-1} are compared as contour plots in Figure 6, together with the corresponding cyclic voltammograms. At the relatively slow cycling rate of 0.5 mV·s^{-1} (Figure 6a) the variation of the strongly adsorbed chemical shift (seen to the right-hand side of the spectra) is well synchronized with the applied voltage. Moreover, a capacitive electrochemical signature with a near rectangular cyclic voltammogram is observed. However, when the cycling rate is increased to 5 mV·s^{-1} (Figure 6b), a considerable lag between the periodic variation of the strongly adsorbed chemical shift and the applied voltage is observed. Indeed, close inspection of the spectra (see inset) shows that between voltages of 0.64 V on charge and 1.66 V of the following discharge, the shift of the strongly adsorbed resonance is found to increase. On the other

dx.doi.org/10.1021/ja410287s | J. Am. Chem. Soc. 2013, 135, 18968−18980

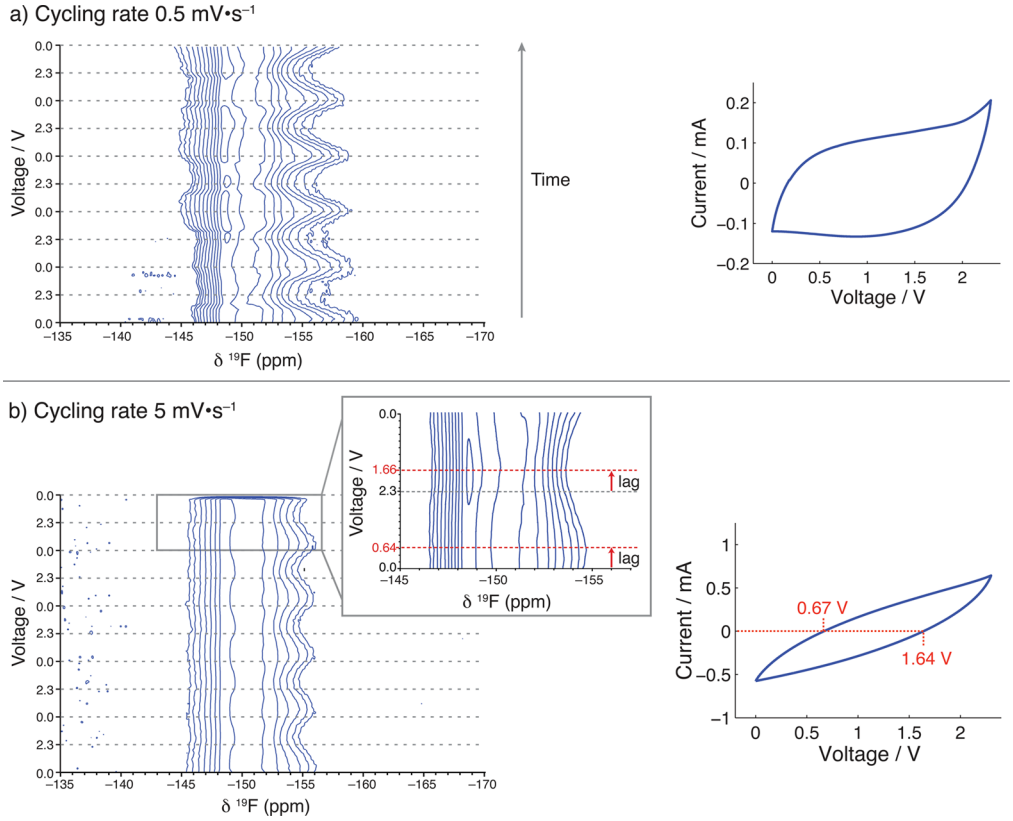

Figure 6. Contour plots of successive in situ ^{19}F NMR spectra of the negative electrode of an overlaid supercapacitor cell with simultaneous cyclic voltammetric cycling. Representative cyclic voltammograms are shown beside the spectra. Spectra and cyclic voltammograms are shown for cycling rates of (a) 0.5 mV·s^{-1} and (b) 5 mV·s^{-1}. In part b, enlarged spectra are shown for the fifth cycle as in inset. For each two-dimensional spectrum, 18 slices were recorded per charging cycle, with recycle intervals of (a) 30 s and (b) 3 s.

hand, between voltages of 1.66 V on discharge and 0.64 V on the next charge cycle, the shift of the strongly adsorbed resonance decreases. This differs from the behavior observed at the lower cycling rate of 0.5 mV·s^{-1}, where the shift of the strongly adsorbed resonance shows only very small lags behind the applied voltage. Inspection of the electrochemistry helps explain this behavior. At the faster cycling rate of 5 mV·s^{-1}, the cyclic voltammogram is far from ideal, with a nonrectangular shape observed. Importantly, positive currents flow between 0.67 V on the charge and 1.64 V on the next discharge, and during this time the magnitude of the charge stored on each electrode increases. However, between voltages of 1.64 V on discharge and 0.67 V on the next charge, a negative current flows and the magnitude of the charge stored at each electrode decreases. The voltages at which the direction of the current reverses agree well with the voltages at which the direction of the shift variation of the adsorbed resonance changes in the real-time in situ NMR spectrum. This confirms that the changes in resonance frequency of the adsorbed resonances are directly correlated with the magnitude of the charge stored on the electrode and not the potential difference applied to the cell. We note that on this basis, the cyclic voltammogram recorded at the slower cycling rate of 0.5 mV·s^{-1} indicates that we should also observe a small lag in the real-time in situ NMR spectrum, since the CV curve is not perfectly rectangular. Indeed, close inspection of the NMR data reveals that a small lag is indeed observed; however, this is found to be on the order of the time taken to record one slice of the two-dimensional data set and so is not readily noticeable in Figure 6a.

3.5. Interpretation of Chemical Shifts for Strongly Adsorbed Species. In the ^{19}F in situ NMR spectra of the BF_4 anions, the resonance corresponding to strongly adsorbed ions is observed to shift to higher frequencies upon charging. This observation is consistent with NMR studies of other nuclei such as ^{13}C and ^{11}B probing both cations and anions in similar systems.[32,50] This suggests that the changes in chemical shift are nucleus-independent and are related to changes in the ring current effects experienced by the nuclei during charging and discharging. Assuming that the observed chemical shift changes are dominated by ring current effects, there are several possible factors that may contribute to the changes in the resonance frequencies observed for adsorbed ions. First, addition or removal of electrons from the carbon electronic structure may modify the ring current effects. Second, during supercapacitor charging cations are expected to become more strongly associated with the negative electrode surface, while anions are expected to become less strongly associated with the negative electrode surface (and vice versa at the positive electrode). The resulting increases or decreases in carbon−ion distances may change the observed chemical shift. Finally, we note that there may be small changes in the carbon micropore sizes during charging and discharging. In situ electrochemical dilatometry revealed small macroscopic height changes of porous carbon electrode films during charging and discharging.[66,67] If these height changes arise from dilation of the carbon micropores as proposed, the effective distance between nuclei in adsorbed molecules and carbon surfaces may again be modified.

dx.doi.org/10.1021/ja410287s | J. Am. Chem. Soc. 2013, 135, 18968−18980

To investigate these effects, DFT calculations were carried out to determine nucleus-independent chemical shifts (NICS) associated with a simple model system. NICS calculations are readily performed using standard quantum mechanics programs whereby isotropic chemical shifts are calculated for "ghost"

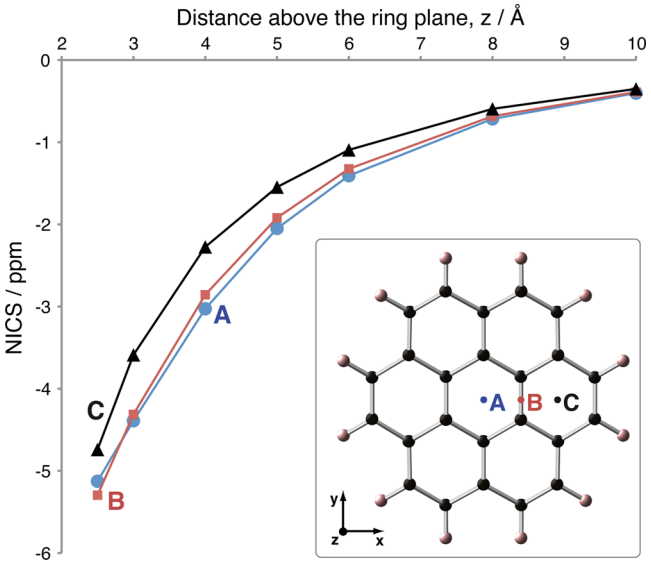

Figure 7. Calculated NICS values above a neutral coronene molecule.

atoms placed at arbitrary positions above and around carbon surfaces. These calculations provide quantification of the effect of ring currents on the resonance frequencies of nuclei situated close to systems containing delocalized electrons. Diatropic (diamagnetic) ring current effects[68] cause shielding fields above the plane of aromatic rings, while paratropic (paramagnetic) ring current effects[69] cause deshielding fields above the plane of antiaromatic rings.[41] Activated carbons have complex amorphous structures consisting of curved graphene sheets,[70] and it is difficult to accurately model these complicated structures in DFT calculations. Recent studies have employed coronene- and fullerene-based structures as simple models for more extended carbon structures.[42,71−73] To explore the origin of the observed NMR frequencies reported in the current work during charging and discharging of supercapacitor electrodes, NICS calculations were performed on the molecule coronene.

Figure 7 shows the calculated NICS as a function of distance above the coronene ring plane for three different positions in the xy plane. The structure of coronene and the positions in the *xy* plane (A, B, and C) for which values were calculated are shown as an inset. A lower limit of 2.5 Å above the coronene ring plane was chosen for calculations, since the approach of an adsorbed molecule and the carbon will be limited by the van der Waals radii of atoms in each. Indeed, the van der Waals radius of sp^2 hybridized carbon is ∼1.7 Å and the van der Waals radii of hydrogen and fluorine are expected to be greater than 1 Å.[74]

For all three positions (A, B, and C) considered, NICS values were calculated to be negative above the ring plane, consistent with diamagnetic ring currents. Moreover, for the three positions considered, NICS values show good agreement with each other, showing that there is an approximately uniform shielding field above coronene. Thus, resonances from adsorbed molecules should appear shielded relative to the corresponding free species. In Figure 2a above we noted that the resonance corresponding to strongly adsorbed BF_4 anions appears at a chemical shift of 5.6 ppm less than the weakly adsorbed anions. This is in reasonable agreement with the NICS value of approximately −5 ppm calculated at 2.5 Å above coronene.

Figure 7 allows us to consider the effect of a nucleus moving closer to, or further away from, a carbon surface. As a nucleus becomes more distant from the coronene surface, the calculated NICS becomes less negative (higher NMR frequency). This in principle could explain the increases in resonance frequency we have observed upon charging (∼3.5 ppm), corresponding to ions moving roughly 6 Å further away from the coronene molecule considered here. While such a distance change may be reasonable for an ion adsorbed on a carbon surface of like charge, the same behavior is not expected for ions adsorbed on carbon surfaces of opposite charge. In this case, charging is expected to reduce the ion−carbon separation due because of electrostatic attraction which would decrease the observed resonance frequency according to the NICS calculations. This is contrary to what is observed in the NMR experiments, where the resonance frequencies of the strongly adsorbed species are always observed to increase during charging, regardless of the electrode studied. It is therefore unlikely that the changes in NMR frequency observed for adsorbed species during charge and discharge arise solely from changes in carbon−ion distances. This is further substantiated by noting that a molecular dynamics study of a supercapacitor comprising porous carbon electrodes showed only small changes of ion−carbon distances (about 0.2 Å) upon charging to a cell voltage of 1 V, although in this case an ionic liquid electrolyte was studied.[23] We also note that the small reversible electrode height changes revealed by electrochemical dilatometry (1.1% and 0.5% for the positive and negative electrodes respectively using YP17 activated carbon and an NEt_4BF_4/ACN electrolyte)[66] are unlikely to have a significant effect on the observed resonance frequencies, as the distance changes would result in a negligible change in the NICS.

To explore the effect of charging on the NICS, calculations were performed on charged coronene molecules. Figure 8 shows NICS plots as a function of distance above the coronene ring plane for three different positions in the *xy* plane (A, B, and C). NICS calculations were performed for optimized coronene molecules with charges of +1*e* (Figure 8a) and −1*e* (Figure 8b), where *e* is the electronic charge.

For both the positively and negatively charged coronene molecules, positive NICS values were calculated for all positions considered above the carbon surface, consistent with paratropic ring currents. The NICS tends toward zero for large distances away from the carbon surface. The calculated increase in resonance frequency for both positively and negatively charged carbon qualitatively agrees with our in situ NMR results, whereby the strongly adsorbed resonance shifts to higher frequencies upon charging in both the positive and negative electrodes. The differences in the magnitudes of the calculated NICSs close to the carbon surface may explain why slightly different changes in resonance frequency are observed in the positive and negative electrodes experimentally, particularly in the low voltage regime. However, the magnitudes of the shifts predicted by the DFT calculations are significantly larger than what we observe experimentally. We note that the model system studied here is a considerable oversimplification of what is expected to be an extended graphene-like pore system in the activated carbon, and so quantitative agreement

dx.doi.org/10.1021/ja410287s | J. Am. Chem. Soc. 2013, 135, 18968−18980

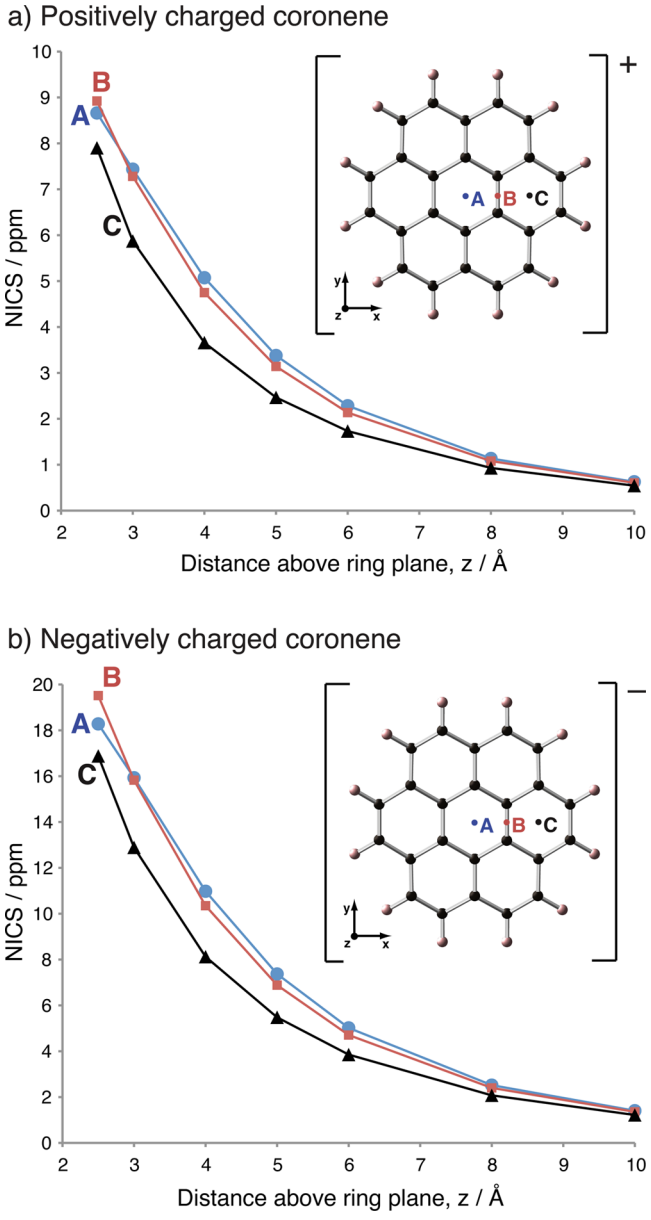

Figure 8. Calculated NICS values above (a) positively and (b) negatively charged coronene.

between the calculated and experimental results is unlikely. Finally, we also note the analogy with the shifts observed in our system with those seen in an early experimental work on [18]annulene. Following two-electron reduction, the ^{1}H chemical shifts of the interior protons changed from −3.0 ppm to 28.1 and 29.5 ppm, explained as arising from the introduction of paratropic ring currents. While changes in carbon−ion distances are still predicted to affect the observed resonance frequencies, the calculations presented here suggest that the introduction of paratropic ring currents by the charge imposed on the carbon will play an important role.

4. CONCLUSIONS

This work has presented a detailed account of the use of NMR for in situ studies of supercapacitors, not only developing the methodology but also revealing fundamental insight into the charge storage mechanism. Specifically, we make two main conclusions for YP50F, an important microporous carbon that is widely used as a supercapacitor electrode material:

(1) Changes in the intensity of the adsorbed resonances in ^{19}F NMR spectra of a YP50F−NEt_4BF_4/dACN supercapacitor system recorded at fixed voltages correspond to changes in the populations of adsorbed BF_4^- species. Analysis of these changes suggests that charging can be divided into at least two distinct regimes. At low cell voltages (less than 0.75 V), the approximately constant anion population in the positive electrode and decreasing anion population in the negative electrode indicate that charging is not dominated by the adsorption of counterions and is instead achieved through short-scale rearrangements and the ejection of co-ions from the micropores. At high cell voltages (greater than 0.75 V), an abrupt increase in the adsorbed anion intensity in the positive electrode, combined with the continued loss of anions from the negative electrode, suggests that both counterion adsorption and co-ion ejection are important in this regime.

(2) Changes in the resonance frequency of the adsorbed species observed during charging arise because of changes in the carbon electronic structure. This effect is external to the electrolyte itself and is therefore independent of the nature of the adsorbed electrolyte species inside the carbon micropores. Indeed, DFT calculations on a simple model system confirm that the addition or removal of electrons to a delocalized system should lead to marked changes in the nucleus-independent chemical shift of nearby species. Importantly, regardless of whether electrons are added or removed from the carbon surface, the DFT calculations predict that a deshielding effect should be observed, in qualitative agreement with our experimental results.

The observation and characterization of these effects open the way for the future study of the supercapacitance phenomenon using NMR. In particular, we envisage that the approaches we have developed will provide insight into the effect of pore size and pore size distribution on the charge storage process. We also note that in principle these methods are applicable to other electrolytes such as ionic liquids, and work is ongoing in our laboratory to investigate these systems.

■ ASSOCIATED CONTENT

Supporting Information

Deconvoluted NMR spectra, deconvolution results from an alternative fitting model, additional cyclic voltammograms of supercapacitors, NMR spectra of free electrolyte samples, cumulated electronic charge in fixed voltage in situ NMR experiments, linear fits of the data in Figure 4c and Figure 4d, and two video files. This material is available free of charge via the Internet at http://pubs.acs.org.

■ AUTHOR INFORMATION

Corresponding Author

cpg27@cam.ac.uk

Author Contributions

‖H.W. and A.C.F. contributed equally to this manuscript.

Notes

The authors declare no competing financial interest.

■ ACKNOWLEDGMENTS

A.C.F., J.M.G., H.W., and C.P.G. acknowledge the Sims Scholarship (A.C.F.), EPSRC (via the Supergen consortium, J.M.G. and H.W.), and the EU ERC (via an Advanced

Fellowship to C.P.G.) for funding. N.M.T. was supported by the Northeastern Center for Chemical Energy Storage and by Energy Frontier Research Center funded by the U.S. DOE, BES under Award No. DE-SC0001294. P.S. acknowledges the support from the European Research Council (ERC, Advanced Grant, ERC-2011-AdG, Project 291543—IONACES). L.T. was supported by the Délégation Générale pour l'Armement. A.C.F. and J.M.G. thank the NanoDTC Cambridge for travel funding. We also thank Yury Gogotsi, Volker Presser, Céline Merlet, and Andy Ilott for useful discussions.

REFERENCES

(1) Simon, P.; Gogotsi, Y. *Nat. Mater.* **2008**, *7*, 845−854.
(2) Miller, J. R.; Simon, P. *Science* **2008**, *321*, 651−652.
(3) Miller, J. R.; Burke, A. *Electrochem. Soc. Interface* **2008**, *17*, 53−57.
(4) Zhai, Y.; Dou, Y.; Zhao, D.; Fulvio, P. F.; Mayes, R. T.; Dai, S. *Adv. Mater.* **2011**, *23*, 4828−4850.
(5) Chmiola, J.; Yushin, G.; Gogotsi, Y.; Portet, C.; Simon, P.; Taberna, P.-L. *Science* **2006**, *313*, 1760−1763.
(6) Chmiola, J.; Largeot, C.; Taberna, P. L.; Simon, P.; Gogotsi, Y. *Angew. Chem., Int. Ed.* **2008**, *47*, 3392−3395.
(7) Lin, R.; Taberna, P. L.; Chmiola, J.; Guay, D.; Gogotsi, Y.; Simon, P. *J. Electrochem. Soc.* **2009**, *156*, A7−A12.
(8) Simon, P.; Gogotsi, Y. *Acc. Chem. Res.* **2013**, *46*, 1094−1103.
(9) Levi, M. D.; Salitra, G.; Levy, N.; Aurbach, D.; Maier, J. *Nat. Mater.* **2009**, *8*, 872−875.
(10) Levi, M. D.; Levy, N.; Sigalov, S.; Salitra, G.; Aurbach, D.; Maier, J. *J. Am. Chem. Soc.* **2010**, *132*, 13220−13222.
(11) Levi, M. D.; Sigalov, S.; Salitra, G.; Elazari, R.; Aurbach, D. *J. Phys. Chem. Lett.* **2011**, *2*, 120−124.
(12) Levi, M. D.; Sigalov, S.; Salitra, G.; Elazari, R.; Aurbach, D.; Daikhin, L.; Presser, V. *J. Phys. Chem. C* **2013**, *117*, 1247−1256.
(13) Boukhalfa, S.; He, L.; Melnichenko, Y. B.; Yushin, G. *Angew. Chem., Int. Ed.* **2013**, *52*, 1−6.
(14) Sharma, K.; Bilheux, H. Z.; Walker, L. M. H.; Voisin, S.; Mayes, R. T.; Kiggans, J. O.; Yiacoumi, S.; DePaoli, D. W.; Dai, S.; Tsouris, C. *Phys. Chem. Chem. Phys.* **2013**, *15*, 11740−11747.
(15) Richey, F. W.; Dyatkin, B.; Gogotsi, Y.; Elabd, Y. A. *J. Am. Chem. Soc.* **2013**, *135*, 12818−12826.
(16) Feng, G.; Cummings, P. T. *J. Phys. Chem. Lett.* **2011**, *2*, 2859−2864.
(17) Feng, G.; Qiao, R.; Huang, J.; Sumpter, B. G.; Meunier, V. *ACS Nano* **2010**, *4*, 2382−2390.
(18) Feng, G.; Qiao, R.; Huang, J.; Dai, S.; Sumpter, B. G.; Meunier, V. *Phys. Chem. Chem. Phys.* **2011**, *13*, 1152−1161.
(19) Shim, Y.; Kim, H. J. *ACS Nano* **2010**, *4*, 2345−2355.
(20) Merlet, C.; Salanne, M.; Rotenberg, B.; Madden, P. A. *J. Phys. Chem. C* **2011**, *115*, 16613−16618.
(21) Merlet, C.; Salanne, M.; Rotenberg, B.; Madden, P. A. *Electrochim. Acta* **2013**, *101*, 262−271.
(22) Merlet, C.; Rotenberg, B.; Madden, P. A.; Salanne, M. *Phys. Chem. Chem. Phys.* **2013**, *15*, 15781−15792.
(23) Merlet, C.; Rotenberg, B.; Madden, P. A.; Taberna, P. L.; Simon, P.; Gogotsi, Y.; Salanne, M. *Nat. Mater.* **2012**, *11*, 306−310.
(24) Kondrat, S.; Kornyshev, A. *J. Phys.: Condens. Matter* **2011**, *23*, 022201.
(25) Kondrat, S.; Georgi, N.; Fedorov, M. V; Kornyshev, A. A. *Phys. Chem. Chem. Phys.* **2011**, *13*, 11359−11366.
(26) Kondrat, S.; Kornyshev, A. *J. Phys. Chem. C* **2013**, *117*, 12399−12406.
(27) Harris, R. K.; Thompson, T. V.; Norman, P. R.; Pottage, C.; Trethewey, A. N. *J. Chem. Soc., Faraday Trans.* **1995**, *91*, 1795−1799.
(28) Harris, R. K.; Thompson, T. V.; Norman, P. R.; Pottage, C. *J. Chem. Soc. Faraday. Trans.* **1996**, *92*, 2615−2618.
(29) Harris, R. K.; Thompson, T. V.; Norman, P. R.; Pottage, C. *Carbon* **1999**, *37*, 1425−1430.
(30) Dickinson, L. M.; Harris, R. K.; Shaw, J. A.; Chinn, M.; Norman, P. R. *Magn. Reson. Chem.* **2000**, *38*, 918−924.
(31) Forse, A. C.; Griffin, J. M.; Wang, H.; Trease, N. M.; Presser, V.; Gogotsi, Y.; Simon, P.; Grey, C. P. *Phys. Chem. Chem. Phys.* **2013**, *15*, 7722−7730.
(32) Wang, H.; Köster, T. K.-J.; Trease, N. M.; Ségalini, J.; Taberna, P.-L.; Simon, P.; Gogotsi, Y.; Grey, C. P. *J. Am. Chem. Soc.* **2011**, *133*, 19270−19273.
(33) Borchardt, L.; Oschatz, M.; Paasch, S.; Kaskel, S.; Brunner, E. *Phys. Chem. Chem. Phys.* **2013**, *15*, 15177−84.
(34) Mitani, S.; Murakami, C.; Korai, Y.; Minato, Y.; Ishimoto, S.; Suematsu, S.; Tamamitsu, K. *Electrochim. Acta* **2013**, *94*, 30−33.
(35) Anderson, R. J.; McNicholas, T. P.; Kleinhammes, A.; Wang, A.; Liu, J.; Wu, Y. *J. Am. Chem. Soc.* **2010**, *132*, 8618−8626.
(36) Liu, X.; Pan, X.; Shen, W.; Ren, P.; Han, X.; Bao, X. *J. Phys. Chem. C* **2012**, *116*, 7803−7809.
(37) Sekhaneh, W.; Kotecha, M.; Dettlaff-Weglikowska, U.; Veeman, W. S. *Chem. Phys. Lett.* **2006**, *428*, 143−147.
(38) Chen, Q.; Herberg, J. L.; Mogilevsky, G.; Wang, H.-J.; Stadermann, M.; Holt, J. K.; Wu, Y. *Nano Lett.* **2008**, *8*, 1902−1905.
(39) Shen, K.; Pietrass, T. *J. Phys. Chem. B* **2004**, *108*, 9937−9942.
(40) Schleyer, P. v. R.; Maerker, C.; Dransfeld, A.; Jiao, H.; Hommes, N. J. R. V. E. *J. Am. Chem. Soc.* **1996**, *7863*, 6317−6318.
(41) Chen, Z.; Wannere, C. S.; Corminboeuf, C.; Puchta, R.; Schleyer, P. v. R. *Chem. Rev.* **2005**, *105*, 3842−3888.
(42) Moran, D.; Stahl, F.; Bettinger, H. F.; Scaefer, H. F., III; Schleyer, P. v. R. *J. Am. Chem. Soc.* **2003**, *125*, 6746−6752.
(43) Mamone, S.; Concistrè, M.; Heinmaa, I.; Carravetta, M.; Kuprov, I.; Wall, G.; Denning, M.; Lei, X.; Chen, J. Y.-C.; Li, Y.; Murata, Y.; Turro, N. J.; Levitt, M. H. *Chem. Phys. Chem.* **2013**, *14*, 3121−30.
(44) Bühl, M. *Chem.—Eur. J.* **1998**, *4*, 734−739.
(45) Sebastiani, D. *Chem. Phys. Chem.* **2006**, *7*, 164−175.
(46) Besley, N. A.; Noble, A. *J. Chem. Phys.* **2008**, *128*, 101102.
(47) Kibalchenko, M.; Payne, M. C.; Yates, J. R. *ACS Nano* **2011**, *5*, 537−545.
(48) Lee, S.-I.; Saito, K.; Kanehashi, K.; Hatakeyama, M.; Mitani, S.; Yoon, S.-H.; Korai, Y.; Mochida, I. *Carbon* **2006**, *44*, 2578−2586.
(49) Azaïs, P.; Duclaux, L.; Florian, P.; Massiot, D.; Lillo-Rodenas, M.-A.; Linares-Solano, A.; Peres, J.-P.; Jehoulet, C.; Béguin, F. *J. Power Sources* **2007**, *171*, 1046−1053.
(50) Deschamps, M.; Gilbert, E.; Azais, P.; Raymundo-Piñero, E.; Ammar, M. R.; Simon, P.; Massiot, D.; Béguin, F. *Nat. Mater.* **2013**, *12*, 351−358.
(51) Blanc, F.; Leskes, M.; Grey, C. P. *Acc. Chem. Res.* **2013**, *46*, 1952−1963.
(52) Trease, N. M.; Zhou, L.; Chang, H. J.; Zhu, B. Y.; Grey, C. P. *Solid State Nucl. Magn. Reson.* **2012**, *42*, 62−70.
(53) Chevallier, F.; Letellier, M.; Morcrette, M.; Tarascon, J.-M.; Frackowiak, E.; Rouzaud, J.-N.; Béguin, F. *Electrochem. Solid State Lett.* **2003**, *6*, A225−A228.
(54) Letellier, M.; Chevallier, F.; Béguin, F.; Frackowiak, E.; Rouzaud, J.-N. *J. Phys. Chem. Solids* **2004**, *65*, 245−251.
(55) Letellier, M.; Chevallier, F.; Morcrette, M. *Carbon* **2007**, *45*, 1025−1034.
(56) Laudisio, G.; Dash, R. K.; Singer, J. P.; Yushin, G.; Gogotsi, Y.; Fischer, J. E. *Langmuir* **2006**, *22*, 8945−8950.
(57) Cory, D. G.; Ritchey, W. M. *J. Magn. Reson.* **1988**, *80*, 128−132.
(58) Massiot, D.; Fayon, F.; Capron, M.; King, I.; Le Calvé, S.; Alonso, B.; Durand, J.-O.; Bujoli, B.; Gan, Z.; Hoatson, G. *Magn. Reson. Chem.* **2002**, *40*, 70−76.
(59) Frisch, M. J.; Trucks, G. W.; Schlegel, H. B.; Scuseria, G. E.; Robb, M. A.; Cheeseman, J. R.; Montgomery, J. A., Jr.; Vreven, T.; Kudin, K. N.; Burant, J. C.; Millam, J. M.; Iyengar, S. S.; Tomasi, J.; Barone, V.; Mennucci, B.; Cossi, M.; Scalmani, G.; Rega, N.; Petersson, G. A.; Nakatsuji, H.; Hada, M.; Ehara, M.; Toyota, K.; Fukuda, R.; Hasegawa, J.; Ishida, M.; Nakajima, T.; Honda, Y.; Kitao, O.; Nakai, H.; Klene, M.; Li, X.; Knox, J. E.; Hratchian, H. P.; Cross, J. B.; Bakken, V.; Adamo, C.; Jaramillo, J.; Gomperts, R.; Stratmann, R. E.; Yazyev, O.; Austin, A. J.; Cammi, R.; Pomelli, C.; Ochterski, J. W.; Ayala, P. Y.; Morokuma, K.; Voth, G. A.; Salvador, P.; Dannenberg, J.

J.; Zakrzewski, V. G.; Dapprich, S.; Daniels, A. D.; Strain, M. C.; Farkas, O.; Malick, D. K.; Rabuck, A. D.; Raghavachari, K.; Foresman, J. B.; Ortiz, J. V.; Cui, Q.; Baboul, A. G.; Clifford, S.; Cioslowski, J.; Stefanov, B. B.; Liu, G.; Liashenko, A.; Piskorz, P.; Komaromi, I.; Martin, R. L.; Fox, D. J.; Keith, T.; Al-Laham, M. A.; Peng, C. Y.; Nanayakkara, A.; Challacombe, M.; Gill, P. M. W.; Johnson, B.; Chen, W.; Wong, M. W.; Gonzalez, C.; Pople, J. A. *Gaussian 03*, revision E.01; Gaussian, Inc.: Wallingford, CT, 2004.

(60) Francke, R.; Cericola, D.; Kötz, R.; Weingarth, D.; Waldvogel, S. R. *Electrochim. Acta* **2012**, *62*, 372−380.

(61) Ulrich, R.; Glaser, R. W.; Ulrich, A. S. *J. Magn. Reson.* **2003**, *164*, 115−127.

(62) Glaser, R. W.; Ulrich, A. S. *J. Magn. Reson. Res.* **2003**, *164*, 104−114.

(63) Zhou, L.; Leskes, M.; Ilott, A. J.; Trease, N. M.; Grey, C. P. *J. Magn. Reson.* **2013**, *234*, 44−57.

(64) Aurbach, D.; Levi, M. D.; Salitra, G.; Levy, N.; Pollak, E.; Muthu, J. *J. Electrochem. Soc.* **2008**, *155*, A745−A753.

(65) Merlet, C.; Péan, C.; Rotenberg, B.; Madden, P. A.; Daffos, B.; Taberna, P.-L.; Simon, P.; Salanne, M. *Nat. Commun.* **2013**, *4*, 2701, DOI: 10.1038/ncomms3701.

(66) Ruch, P. W.; Kötz, R.; Wokaun, A. *Electrochim. Acta* **2009**, *54*, 4451−4458.

(67) Hantel, M. M.; Presser, V.; Kötz, R.; Gogotsi, Y. *Electrochem. Commun.* **2011**, *13*, 1221−1224.

(68) Pople, J. A. *J. Chem. Phys.* **1956**, *24*, 1111.

(69) Pople, J. A. *J. Am. Chem. Soc.* **1966**, 1−5.

(70) Harris, P. *Crit. Rev. Solid State Mater. Sci.* **2005**, *30*, 235−253.

(71) Popov, I. A.; Bozhenko, K. V; Boldyrev, A. I. *Nano Res.* **2012**, *5*, 117−123.

(72) Vähäkangas, J.; Ikäläinen, S.; Lantto, P.; Vaara, J. *Phys. Chem. Chem. Phys.* **2013**, *15*, 4634−4641.

(73) Deschamps, M.; Cadars, S.; Gilbert, E.; Azaïs, P.; Raymundo-Pinero, E.; Béguin, F.; Massiot, D. *Solid State Nucl. Magn. Reson.* **2012**, *42*, 81−86.

(74) Bondi, A. *J. Phys. Chem.* **1965**, *68*, 441−451.